Geochimica et Cosmochimica Acta, Vol. 69, No. 14, pp. 3631–3642, 2005

0016-7037/05 $30.00 + .00

ELSEVIER

doi:10.1016/j.gca.2005.02.031

High-resolution $\delta^{13}C$ intratooth profiles in bovine enamel: Implications for mineralization pattern and isotopic attenuation

ANTOINE ZAZZO,[1,2,*] MARIE BALASSE,[3] and WILLIAM P. PATTERSON[1]

[1]Department of Geological Sciences, University of Saskatchewan, 114 Science Place, Saskatoon, SK S7N 5E2, Canada
[2]CNRS UPR 2147, 44 rue de l'Amiral Mouchez, 75014 Paris, France
[3]CNRS UMR 5197, Muséum national d'Histoire naturelle, Département Ecologie et Gestion de la Biodiversité, 55 rue Buffon, Paris 75231, France

(*Received September* 14, 2004; *accepted in revised form February* 24, 2005)

Abstract—We present the first high-resolution carbon isotope and carbonate content profiles generated through the thickness of enamel from a steer fed C_3- then C_4-dominant food. Carbonate contents decrease by ~2 wt% from the enamel surface to the innermost enamel layer, and each carbon isotope profile shows a mixture of enamel portions mineralized over several months. Downward and outward increasing contribution of C_4 food to the enamel $\delta^{13}C$ values reveal two components of the mineralization gradient: a vertical component from the tip of the tooth crown to the neck, and a horizontal component from the enamel-dentine junction to the outer enamel. We use our results to infer mineralization parameters for bovines and to calculate expected isotopic attenuations for an array of environmental inputs and microsampling strategies, using the model developed by Passey and Cerling [*Geochim. Cosmochim. Acta.* 66 (2002) 3225–3234]. Although it seems unlikely that any strategy will perfectly isolate discrete time slices, sampling the innermost enamel layer might offer the advantage of significantly reducing the isotope damping that would become independent of the structure of the input signal. *Copyright © 2005 Elsevier Ltd*

1. INTRODUCTION

Stable isotope geochemistry has been extensively used to reconstruct rapid change in animal dietary habits, migration patterns, or past climate from hypsodont (high-crowned) tooth enamel (e.g., Fricke and O'Neil, 1996; Kohn et al., 1998; Sharp and Cerling, 1998; Gadbury et al., 2000; Balasse et al., 2002; Zazzo et al., 2002). In mammals like bovids and equids, tooth formation proceeds from the tip of the tooth crown (apex) to the neck (cervix) as teeth emerge, and tooth enamel is not remodeled once formed. As a result, enamel records environmental- and climatic-constrained changes in the isotope value of water or food ingested during tooth mineralization.

Pioneer work implicitly assumed that enamel grows by adding new material perpendicular to the tooth length axis, and that discrete amounts of time could be extracted from each individual tooth subsample. Serial microsamples have been collected by drilling or cutting segments perpendicular to the tooth length axis, each sample crossing all of the enamel thickness. But amelogenesis (tooth enamel formation) is a two-step process beginning with the rapid deposition of an organic-rich, mineral-poor matrix followed by a phase of progressive maturation that produces the fully mineralized enamel (Weinmann et al., 1942; Suga et al., 1970, 1987; Suga, 1979, 1982; Sakae and Hirai, 1982; Moss-Salentijn et al., 1997). During the maturation stage, Suga (1979, 1982) reported three mineralization fronts advancing in various directions, some of them subparallel to the enamel-dentine junction. Therefore, the amount of time required for completing mineralization might far exceeds the time of tooth growth. Consequently, instead of representing discrete time slices, each enamel subsample extracted following the conventional method mixes enamel portions that were mineralized over a long period of time. This sampling strategy likely results in biases for reconstructing environmental and climatic variations.

As scientists became aware of this, the question arose as to how much time is actually represented by each horizontal tooth subsample. Determination of precise timing and geometry of enamel mineralization became critical for designing new collecting strategies and for modeling purposes (Fisher and Fox, 1998; Balasse, 2002, 2003; Passey and Cerling, 2002). Unfortunately, incremental features in enamel (Retzius' striae, daily cross-striations) are not helpful for establishing more appropriate microsampling procedures because they form during the stage of matrix deposition, when little mineralization occurs. No visible growth feature is preserved from the maturation stage, and only radiographs of thin sections taken from developing teeth (Brown et al., 1960; Hoppe et al., 2004), or isotopic labeling (Balasse et al., 2001; Balasse ,2002), can help delineate the precise timing and geometry of enamel mineralization.

Passey and Cerling (2002) presented a model that describes enamel mineralization in ungulates with ever-growing teeth. This model may be used to correct for the attenuation of the environmental isotopic signal occurring when using the conventional sampling procedure. This model, however, may not fully consider the complexity of the mineralization process (Brown, 1960; Suga, 1979, 1982; Hoppe et al., 2004). It is also unclear whether the model can accurately predict attenuation factors for hypsodont teeth with definite growth, which can only be tested by experiment. In addition, a better understanding of the spatial organization of enamel mineralization might help to establish the most appropriate microsampling strategy for optimizing the time resolution of sampling, and perhaps quantify the amount of time represented in each subsample.

* Author to whom correspondence should be addressed (antoine.zazzo@usask.ca).

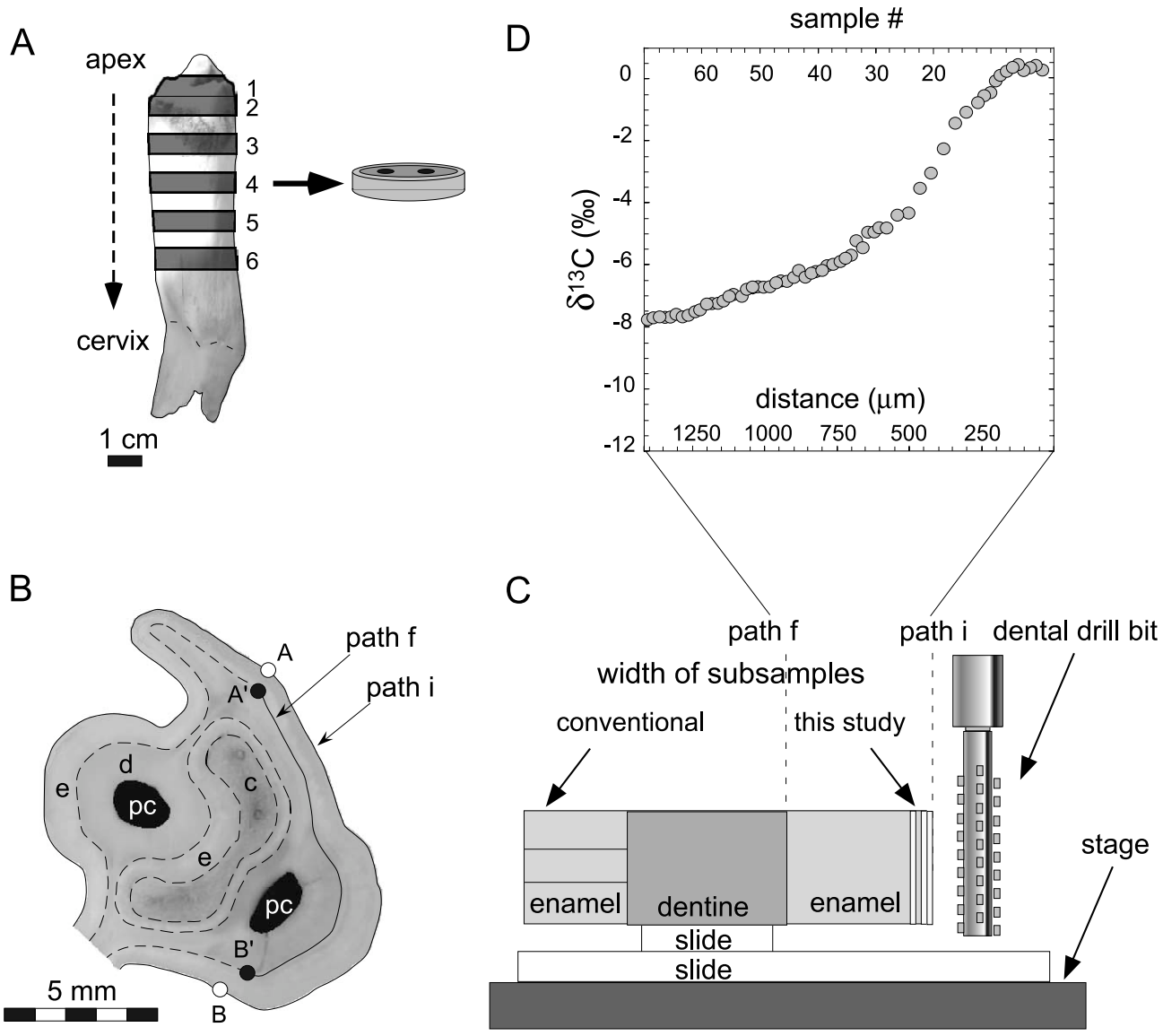

Fig. 1. Schematic representation of the microsampling procedure. (A) Preparation of the 3-mm-thick tooth slices. (B) Two-dimensional representation of tooth slice and manually selected three-dimensional coordinates along outer enamel surface (path i) and enamel-dentine junction (path f). e: Enamel; d: dentine; pc: pulp cavity; c: cement. (C) Sampling device. Note that sampling width is much smaller than drill width. A schematic representation of conventional procedure is also given for comparison. (D) High-resolution $\delta^{13}C$ profile measured in tooth enamel (distance from enamel surface).

This study represents an additional effort at addressing the problem of attenuation of environmental isotopic signals in growing enamel. Here we present the results of an experiment on steers (*Bos taurus*) fed C_3- then C_4-dominant food. Diets were changed during the tenth month of the animals' life and the resulting isotopic change was recorded in their second molars. For the first time, micromilling techniques were used to explore the impact of the mineralization process on enamel isotope value at the micrometer scale, to produce a two-dimensional map of the enamel carbon isotope value. Coupling natural labeling with high precision microsampling should allow us to (1) test if the model presented by Passey and Cerling (2002) for ever growing teeth is applicable to bovid teeth with definite growth and (2) investigate whether alternative microsampling strategies might allow more accurate representation of environmental records to be reconstructed.

2. MATERIALS AND METHODS

2.1. Material

This study was conducted on five steers (*Bos taurus*) raised on an experimental farm (Ferme Expérimentale des Etablières, Vendée, France), where diet was carefully controlled throughout life. Detailed records of diet management and composition were previously published, together with results from previous investigations on the isotopic record of diet change in the jawbone and teeth of the individuals (Balasse et al., 1999; Balasse et al., 2001; Balasse, 2002). Calves were raised on a C_3-based milk diet during the first 9–10 months of life (lactating cows were fed C_3 grass $\delta^{13}C_{grass} = -26.5‰$ VPDB). At weaning, they were switched to a C_4-dominated diet (maize), and

Table 1. $\delta^{13}C$ values of horizontal enamel subsamples extracted from the second molars of five steer following the conventional sampling method. Low-resolution sampling (each sample spanning 4 mm) and isotope analyses are from Balasse (2002), and numbers between brackets represent Balasse's (2002) sample numbers. A higher resolution sampling (every millimeter) was performed on V3 for the interlaboratory calibration in this study.

V2 (h = 53 mm)			V3 (h = 48 mm)				
distance from apex (mm)	(#)	$\delta^{13}C$ (V-PDB, ‰)	distance from apex (mm)	(#)	$\delta^{13}C$ (V-PDB, ‰)	distance from apex (mm)	$\delta^{13}C$ (V-PDB, ‰)
0.0–2.5	(1)	−9.7	0.0–3.5	(1)	−12.2	7.3–8.2	−10.6
2.5–7.0	(2)	−8.6	3.5–6.5	(2)	−11.3	8.2–9.1	−11.2
7.0–11.5	(3)	−7.1	6.5–10.5	(3)	−9.3	9.1–10.1	−9.9
11.5–16.0	(4)	−5.4	10.5–14.0	(4)	−7.1	14.3–15.1	−6.9
16.0–20.5	(5)	−4.0	14.0–17.0	(5)	−6.2	15.1–15.9	−6.6
20.5–24.5	(6)	−3.9	17.0–21.0	(6)	−4.4	15.9–17.1	−6.3
24.5–28.5	(7)	−3.8	21.0–25.5	(7)	−2.6	28.3–29.1	−1.6
28.5–32.5	(8)	−3.9	25.5–30.0	(8)	−1.5	29.1–29.9	−1.4
32.5–36.5	(9)	−3.4	30.0–34.0	(9)	−1.1	29.9–30.9	−1.8
36.5–40.5	(10)	−3.6	34.0–38.0	(10)	−1.1	35.1–36.0	−1.5
40.5–44.5	(11)	−3.8	38.0–42.0	(11)	−0.8	36.0–36.9	−1.2
44.5–48.5	(12)	−3.7	42.0–46.0	(12)	−0.7	36.9–37.9	−0.8

V4 (h = 51 mm)			V5 (h = 48 mm)			V6 (h = 50 mm)		
distance from apex (mm)	(#)	$\delta^{13}C$ (V-PDB, ‰)	distance from apex (mm)	(#)	$\delta^{13}C$ (V-PDB, ‰)	distance from apex (mm)	(#)	$\delta^{13}C$ (V-PDB, ‰)
0.0–2.5	(1)	−13.3	0.0–2.5	(1)	−11.9	0.0–2.0	(1)	−13.0
2.5–6.5	(2)	−11.9	2.5–7.0	(2)	−10.0	2.0–6.0	(2)	−11.8
6.5–10.5	(3)	−11.1	7.0–11.5	(3)	−7.9	6.0–10.0	(3)	−10.7
10.5–14.5	(4)	−10.0	11.5–16.0	(4)	−5.9	10.0–14.0	(4)	−9.0
14.5–18.5	(5)	−9.0	16.0–20.0	(5)	−4.1	14.0–18.0	(5)	−7.7
18.5–22.5	(6)	−7.7	20.0–24.5	(6)	−2.1	18.0–22.0	(6)	−6.8
22.5–26.5	(7)	−6.3	24.5–29.0	(7)	−1.2	22.0–25.0	(7)	−5.5
30.5–34.5	(9)	−2.6	29.0–33.5	(8)	−0.7	25.0–29.0	(8)	−4.7
34.5–38.5	(10)	−2.5	33.5–38.0	(9)	−0.5	29.0–33.0	(9)	−4.1
38.5–42.5	(11)	−2.5	38.0–42.5	(10)	−0.3	33.0–37.0	(10)	−3.6
42.5–46.5	(12)	−2.4	42.0–45.5	(11)	0.1	37.0–40.0	(11)	−3.7
46.5–50.5	(13)	−2.5				40.0–44.0	(12)	−3.7
						44.0–48.0	(13)	−3.5

therefore the diet switch occurred during the formation of the second molar. Individuals labeled V3 and V5 were kept in stall 5, with maize providing 89% by weight of the total dietary carbon (estimated $\delta^{13}C_{diet}$ = −13.4‰ VPDB). Individuals labeled V2, V4, and V6 were kept in stall 6, with maize providing 63% by weight of the total dietary carbon (estimated $\delta^{13}C_{diet}$ = −17.0‰). The animals were killed eight months after the introduction of C_4 plants to their diet, at age 17–18 months (Balasse et al., 1999).

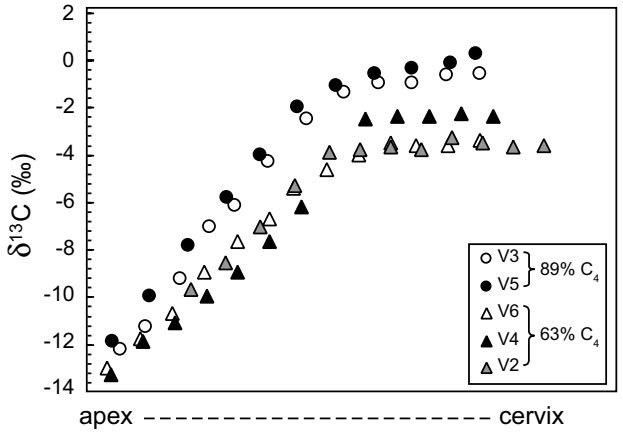

Fig. 2. Intratooth carbon isotope variation of enamel apatite along the second lower molar of the experimental steer (data from Balasse, 2002). The profile from individual V2 was out of phase and shifted by 10 mm to fit the other profiles. This could be due to variability in the timing of tooth mineralization between individual bovids.

2.2. Microsampling Procedure

Microsampling was performed on one lobe from the lower second molar of individual V3 (V3M2). Six slices were cut perpendicular to the growth axis of the tooth using a diamond saw (Fig. 1). The thickness of each slice is 2.7–2.9 mm. Slices were glued to glass slides, with the portion of the tooth being sampled overlapping the edge of the slide. The glass side was then glued to a second glass slide that was fixed to the micromilling stage beneath a stationary diamond dental drill. Powder was recovered on weighing paper placed between the two glass slides during microsampling. Tooth slices were micromilled following the methodology described in Wurster et al. (1999). For each slice, two paths, one on the outer enamel surface (path i) and the other at the enamel-dentine junction (EDJ, path f), were digitized as a series of three-dimensional coordinates, and "smoothed" intermediate coordinates were interpolated by cubic spline. Sixty to seventy intermediate sampling paths were calculated at every 20 μm between the two digitized curves, and were micromilled using the edge of a diamond dental drill. This methodology allows for subsamples to be taken contiguously at a spatial resolution that is only constrained by the precision of the step size (0.05 μm) rather than drill width as in conventional sampling. Powder from each micromilled enamel subsample was collected along the height of the tooth slice, and therefore

Table 2. Carbon isotope values ($\delta^{13}C$) and carbonate content ($[CO_3^{2-}]$) across the enamel thickness of six horizontal tooth slices from V3M2. Positions are expressed as the distance from the outer enamel surface.

V3M2-1			V3M2-2			V3M2-3		
position (mm)	$[CO_3^{2}]$ (wt%)	$\delta^{13}C$ (‰)	position (mm)	$[CO_3^{2}]$ (wt%)	$\delta^{13}C$ (‰)	position (mm)	$[CO_3^{2}]$ (wt%)	$\delta^{13}C$ (‰)
0.00–0.02	3.2	−6.7	0.00–0.03	—	−4.9	0.00–0.08	3.3	−2.6
0.02–0.03	3.2	−7.1	0.03–0.09	—	−5.0	0.08–0.10	2.8	−2.8
0.03–0.07	3.7	−5.9	0.09–0.12	3.6	−5.8	0.10–0.12	3.8	−3.3
0.07–0.11	3.8	−6.8	0.12–0.14	3.2	−7.2	0.12–0.14	3.5	−3.9
0.11–0.15	3.5	−7.6	0.14–0.18	3.5	−8.0	0.14–0.16	3.7	−4.7
0.15–0.19	4.0	−8.0	0.18–0.20	2.7	−8.8	0.16–0.18	3.2	−4.9
0.19–0.23	4.0	−8.3	0.20–0.22	2.9	−8.9	0.18–0.20	3.3	−5.4
0.23–0.27	4.0	−8.8	0.22–0.24	2.5	−9.2	0.20–0.22	3.1	−5.6
0.27–0.31	4.2	−9.7	0.24–0.26	4.2	−9.2	0.22–0.24	3.2	−5.7
0.31–0.35	4.2	−10.0	0.28–0.30	4.0	−9.6	0.26–0.28	—	−6.1
0.39–0.39	4.2	−10.6	0.32–0.34	3.4	−9.8	0.30–0.32	3.0	−6.3
0.39–0.43	4.0	−10.9	0.36–0.39	4.4	−10.1	0.34–0.36	—	−6.5
0.43–0.47	4.4	−11.8	0.41–0.43	4.2	−10.3	0.38–0.40	3.4	−6.6
0.47–0.51	4.6	−12.1	0.45–0.47	3.8	−10.5	0.42–0.44	—	−7.0
0.51–0.55	—	−12.3	0.49–0.51	—	−10.7	0.46–0.48	4.0	−7.0
0.55–0.59	4.5	−12.4	0.53–0.55	4.7	−10.9	0.50–0.52	4.1	−7.2
0.59–0.63	4.1	−12.7	0.57–0.59	4.0	−10.9	0.54–0.56	3.3	−7.3
0.63–0.67	4.2	−12.5	0.61–0.63	4.9	−11.0	0.58–0.60	3.5	−7.3
0.67–0.71	—	−12.6	0.65–0.67	4.8	−11.0	0.62–0.64	4.3	−7.4
0.71–0.75	4.4	−12.6	0.69–0.71	—	−11.0	0.66–0.68	4.5	−7.5
0.75–0.79	4.5	−12.7	0.73–0.75	4.5	−10.9	0.70–0.72	—	−7.7
0.79–0.83	3.6	−12.7	0.77–0.79	4.5	−10.9	0.74–0.76	4.6	−7.6
0.83–0.87	4.5	−12.9	0.81–0.83	4.0	−11.0	0.78–0.80	—	−7.6
0.87–0.91	—	−13.1	0.85–0.87	4.5	−11.0	0.82–0.84	4.9	−7.5
0.91–0.95	4.5	−13.1	0.87–0.89	4.5	−10.9	0.86–0.88	3.8	−7.2
0.95–0.99	4.6	−13.1	0.93–0.95	4.8	−11.0	0.90–0.92	4.9	−7.1
0.99–1.02	4.6	−13.1	0.99–1.01	5.1	−11.1	0.94–0.96	4.5	−7.1
1.02–1.06	4.9	−13.1	1.01–1.03	4.3	−11.1	0.98–1.00	—	−7.0
1.06–1.10	—	−13.2	1.05–1.07	3.9	−11.1	1.02–1.04	4.5	−6.8
1.10–1.14	5.1	−13.2	1.09–1.11	4.0	−11.2	1.06–1.08	4.1	−6.8
1.14–1.18	5.0	−13.2	1.13–1.15	4.6	−11.1	1.08–1.10	—	−6.7
1.18–1.22	4.9	−13.2	1.15–1.17	4.3	−11.1	1.10–1.12	—	−6.8
1.22–1.26	5.2	−13.2	1.17–1.20	4.8	−11.2	1.12–1.14	5.1	−6.7
1.26–1.30	5.1	−13.0	1.20–1.22	4.9	−11.3	1.14–1.16	5.2	−6.6
1.30–1.34	5.2	−13.3	1.22–1.24	5.0	−11.4	1.16–1.18	4.0	−6.7
1.34–1.38	5.1	−13.2	1.24–1.26	4.5	−11.3	1.18–1.20	4.2	−6.6
			1.26–1.28	5.1	−11.4			
			1.28–1.30	5.0	−11.5			

V3M2-4			V3M2-5			V3M2-6		
position (mm)	$[CO_3^{2}]$ (wt%)	$\delta^{13}C$ (‰)	position (mm)	$[CO_3^{2}]$ (wt%)	$\delta^{13}C$ (‰)	position (mm)	$[CO_3^{2}]$ (wt%)	$\delta^{13}C$ (‰)
0.00–0.04	2.3	0.2	0.00–0.02	3.7	0.4	0.00–0.10	3.3	−0.7
0.04–0.06	2.6	0.4	0.00–0.02	—	−0.2	0.10–0.14	3.2	−0.4
0.06–0.08	3.2	0.3	0.02–0.06	3.5	0.0	0.14–0.16	3.5	−0.5
0.08–0.10	3.3	0.3	0.06–0.10	3.4	0.4	0.16–0.18	3.5	−0.4
0.10–0.12	3.4	0.4	0.08–0.12	3.8	0.5	0.18–0.20	3.5	−0.5
0.12–0.14	3.3	0.3	0.12–0.14	3.2	0.2	0.20–0.22	3.6	−0.5
0.14–0.16	3.6	0.2	0.14–0.16	3.6	0.0	0.22–0.24	3.7	−0.7
0.16–0.18	3.6	0.1	0.16–0.18	3.5	−0.1	0.24–0.26	3.7	−0.7
0.18–0.20	3.7	−0.1	0.18–0.20	—	−0.4	0.26–0.28	3.8	−0.8
0.20–0.22	3.7	−0.5	0.20–0.22	4.2	−0.4	0.28–0.30	3.8	−0.9
0.22–0.24	3.5	−0.6	0.22–0.24	4.6	−0.4	0.30–0.32	4.0	−0.9
0.24–0.26	3.7	−0.8	0.24–0.26	4.0	−0.3	0.32–0.34	4.0	−0.9
0.28–0.30	4.1	−1.1	0.26–0.28	3.8	−0.5	0.38–0.40	4.1	−1.0
0.32–0.34	4.0	−1.5	0.28–0.30	3.9	−0.4	0.42–0.44	4.1	−1.0
0.36–0.38	4.0	−2.3	0.30–0.32	3.7	−0.5	0.46–0.48	4.1	−1.1
0.40–0.42	4.1	−3.1	0.36–0.38	4.1	−0.7	0.50–0.52	4.0	−1.2
0.44–0.46	3.9	−3.6	0.42–0.44	4.1	−0.8	0.54–0.56	4.3	−1.2
0.48–0.50	4.4	−4.4	0.48–0.50	4.4	−0.9	0.58–0.60	4.2	−1.2
0.52–0.54	4.5	−4.4	0.53–0.55	4.0	−1.1	0.62–0.64	4.3	−1.3
0.56–0.58	4.7	−4.8	0.59–0.61	4.6	−1.1	0.65–0.67	4.3	−1.3
0.58–0.60	4.5	−4.8	0.63–0.65	5.1	−1.2	0.69–0.71	4.4	−1.3

Table 2. (Continued)

V3M2-4			V3M2-5			V3M2-6		
position (mm)	$[CO_3^2]$ (wt%)	$\delta^{13}C$ (‰)	position (mm)	$[CO_3^2]$ (wt%)	$\delta^{13}C$ (‰)	position (mm)	$[CO_3^2]$ (wt%)	$\delta^{13}C$ (‰)
0.60–0.62	4.5	−5.0	0.69–0.71	4.9	−1.4	0.73–0.75	4.2	−1.3
0.62–0.64	3.9	−5.0	0.75–0.77	4.6	−1.8	0.77–0.79	4.5	−1.3
0.64–0.66	4.3	−5.5	0.81–0.83	4.8	−2.5	0.81–0.83	4.5	−1.3
0.66–0.68	4.4	−5.2	0.85–0.87	5.0	−3.0	0.85–0.87	4.5	−1.3
0.68–0.70	4.0	−5.7	0.89–0.91	4.9	−4.1	0.89–0.91	4.2	−1.2
0.70–0.72	4.0	−5.8	0.93–0.95	5.6	−4.6	0.93–0.95	4.5	−1.2
0.72–0.74	4.2	−5.9	0.97–0.99	4.9	−5.8	0.97–0.99	4.3	−1.1
0.74–0.76	4.5	−6.0	0.99–1.01	5.0	−6.2	1.01–1.03	4.3	−1.1
0.76–0.78	4.5	−6.1	1.01–1.03	5.4	−6.5	1.05–1.07	4.6	−1.2
0.78–0.80	4.6	−6.2	1.03–1.05	5.2	−6.7	1.09–1.11	4.7	−1.2
0.80–0.82	4.6	−6.2	1.05–1.07	—	−6.7	1.13–1.15	4.5	−1.2
0.82–0.84	4.5	−6.3	1.07–1.09	5.2	−7.0	1.17–1.19	5.1	−1.1
0.84–0.86	5.0	−6.4	1.09–1.11	5.2	−7.2	1.21–1.23	5.0	−1.2
0.86–0.88	4.6	−6.2				1.25–1.27	4.5	−1.3
0.88–0.90	4.5	−6.4						
0.90–0.92	4.7	−6.5						
0.92–0.94	4.3	−6.6						
0.94–0.96	4.7	−6.6						
0.96–0.98	4.6	−6.7						
0.98–1.00	5.0	−6.7						
1.00–1.02	5.1	−6.7						
1.02–1.04	4.9	−6.8						
1.04–1.06	5.3	−6.8						
1.06–1.08	5.3	−7.1						
1.08–1.10	5.2	−7.0						
1.10–1.12	5.3	−7.1						
1.12–1.14	4.6	−7.2						
1.14–1.16	5.4	−7.3						
1.16–1.18	5.3	−7.3						
1.18–1.20	5.0	−7.3						
1.20–1.22	5.3	−7.5						
1.22–1.24	5.1	−7.5						
1.24–1.26	5.1	−7.7						
1.26–1.28	5.4	−7.7						
1.28–1.30	5.6	−7.6						
1.32–1.34	5.8	−7.7						
1.34–1.36	5.8	−7.7						
1.36–1.38	5.7	−7.8						
1.38–1.40	5.7	−7.8						
1.40–1.42	5.6	−7.8						

represents a significant volume of ~20 × 0.02 × 3 mm (l × w × h). This modification was necessary to collect sufficient powder for isotopic analyses, but was also likely to be responsible for some spatial averaging (see 2.3). The milled apatite powder was collected manually with a razor blade.

We also milled subsamples from four of the six slices following the conventional sampling method. In each slice, the thickness was split in three, so that each subsample had a volume of ~1 × 1 × 1 mm, spanning the total enamel thickness (Fig. 1B and C). This additional sampling was performed for interlaboratory calibration purposes and to avoid any methodologic bias when comparing our results with those published in Balasse (2002) for the second lobe of the same tooth.

2.3. Isotopic Analyses

Samples were roasted under vacuum for 2 h at 200°C. This additional step permits detection of dentine in the subsample by turning organic matter brown: organic matter in dentine is ~30% by weight as compared with less than 1% in enamel. If the path is not parallel to the two main boundaries (i.e., the enamel surface and the EDJ), the subsampled $\delta^{13}C$ value will not represent an average of the tooth height, but will rather overestimate the upper or the lower part of the slice. Close to the EDJ, some mixing of enamel and dentine can occur, and the transition from 100% enamel to 100% dentine spans five consecutive subsamples (100 μm thick). Based on this observation, and although sampling path is 20 μm, we estimate our "effective" sampling precision to be probably closer to 100 μm, but this can vary from one profile to another, depending on the geometry of the slice. Even with this limitation in mind, our precision is likely better than in situ microlaser sampling methods that generate ablation pits of 100 μm diameter with halos extending outward another 100–200 μm (Sharp and Cerling, 1996).

Between 34 and 61 samples are analyzed per slice. The last sample from a profile is the one that remains white after heating which marks the enamel-dentine contact. About 500 μg of each enamel subsample was weighed and reacted in a Kiel III carbonate device interfaced to a Finnigan MAT 253 isotope ratio mass spectrometer in the Saskatchewan Isotope Laboratory, University of Saskatchewan. Carbon dioxide was generated by reaction of apatite carbonate with four drops of anhydrous phosphoric acid in individual reaction vessels at 70°C for five minutes. The carbonate content of each sample was determined by coulometry during acid digestion with an analytical precision of ±0.3 wt% (1σ). Analytical precision for carbon isotopic analyses is ±0.03‰ (1σ), determined from replicate analyses of the Miocene phosphorite NBS120c ($\delta^{13}C$ = −6.32‰, n = 7). Isotopic measurements were normalized to daily

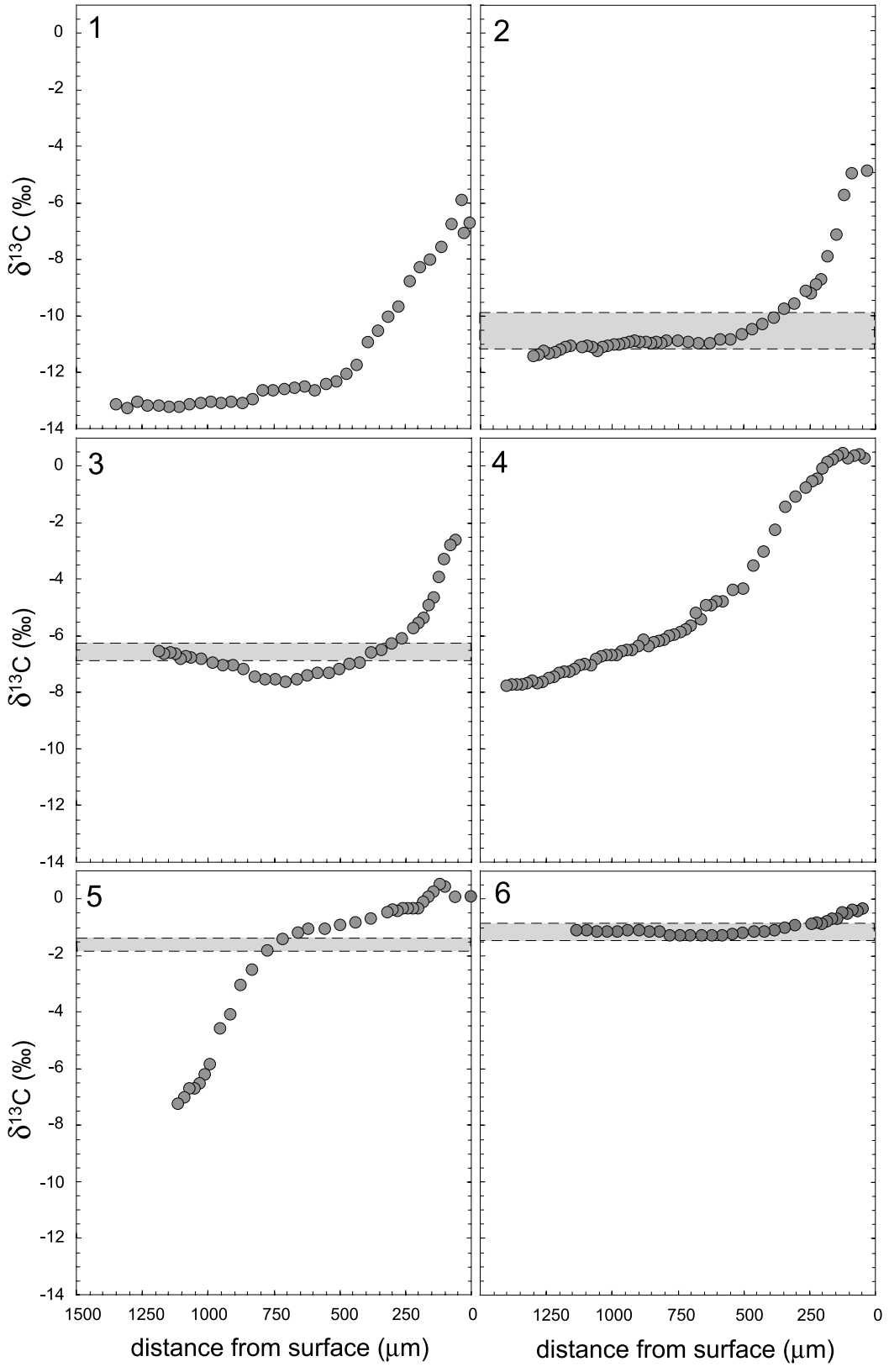

Fig. 3. High-resolution carbon isotope profiles across the enamel thickness of the second molar of individual V3. Series are plotted from enamel-dentine junction to outer enamel surface. Profiles are plotted from apex (1) to cervix (6).

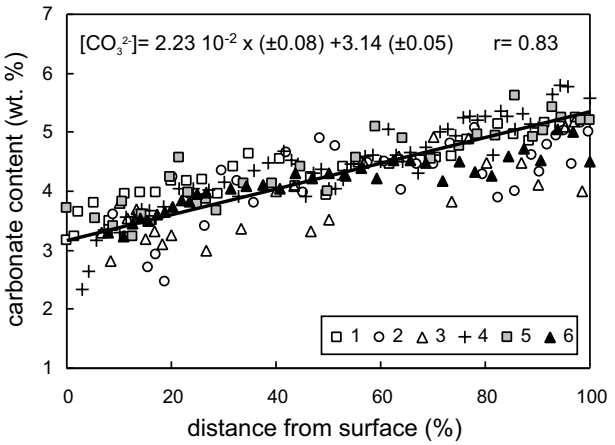

Fig. 4. High-resolution carbonate content profiles across the enamel thickness of the second molar of individual V3. Series are plotted from enamel-dentine junction to outer enamel surface. Profiles are plotted from apex (1) to cervix (6).

analyses of the international standards NBS-18 and NBS-19. $\delta^{13}C$ analyses are reported in the permil notation relative to VPDB.

3. RESULTS

Carbon isotope values from hand-milled subsamples in individuals V2 to V6 using the conventional sampling method are presented in Table 1 and Figure 2. Our results obtained on V3M2 mimic those from Balasse (2002) performed on the other lobe from the same specimen (Table 2), indicating that isotope profiles obtained in both laboratories can be directly compared. As observed in Balasse (2002), the sudden change in diet is reflected by a progressive increase in $\delta^{13}C$ values along the tooth length axis. The upper part of the crown has $\delta^{13}C$ values that are between $-12‰$ and $-13‰$, typical for a C_3 diet. Carbon isotope values of the tooth increase downward in the tooth to plateau in the lower third of the crown. Maximum $\delta^{13}C$ values are proportional to the C_4 content of their diet. Individuals V2, V4, and V6, whose new diet contained 63% C_4 carbon

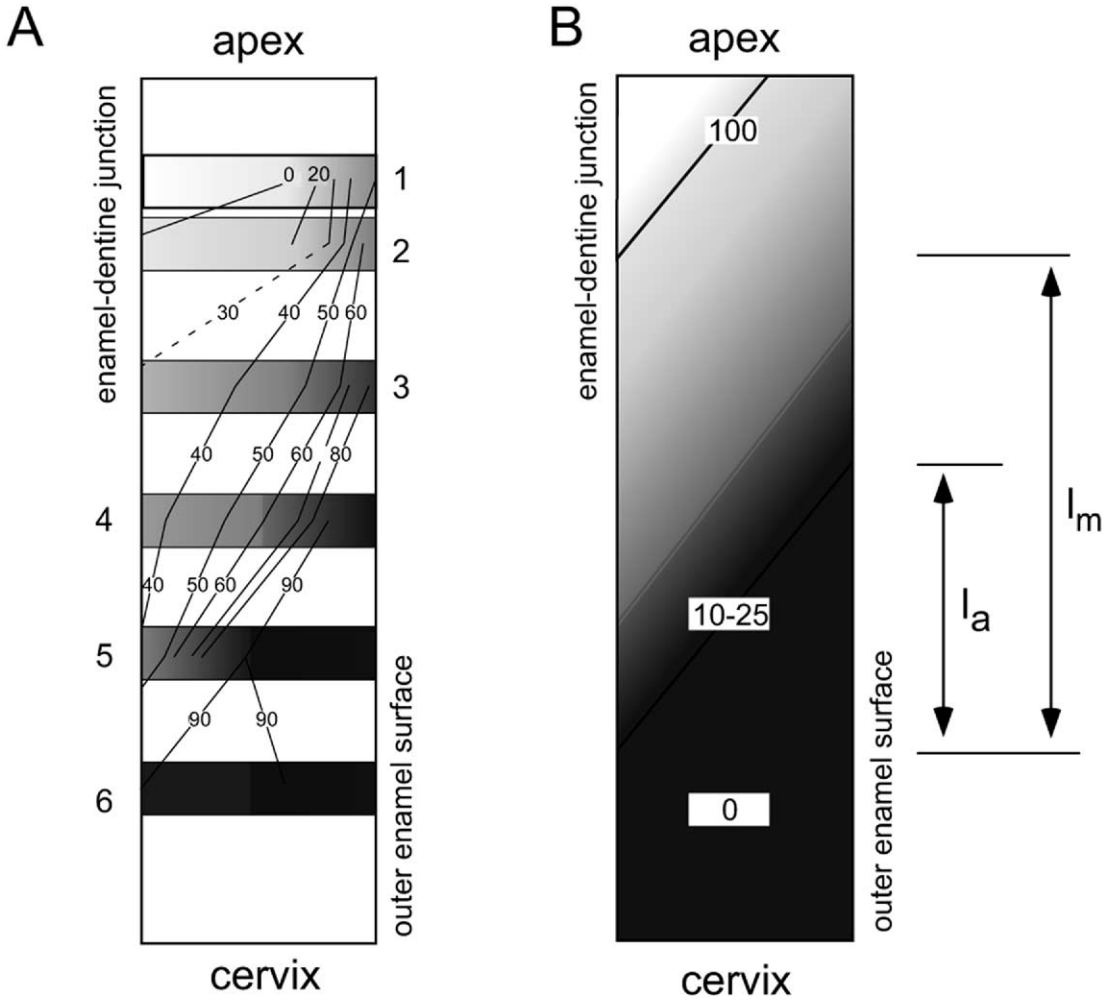

Fig. 5. (A) Two-dimensional mapping of V3M2 carbon isotope values. Percentages of C_4 contribution to enamel $\delta^{13}C$ values are calculated based on a linear mixing model between C_3 and C_4 diet with values of $-26.5‰$ and $-13.4‰$, respectively, and an enrichment factor of 13.5‰ between diet and apatite. (B) Schematic diagram of the steer second molar, showing the model parameters l_a and l_m used in Eqns. 1 and 2. Mineral content (numbers) and location of the appositional front are shown at the time of diet switch (day 295). Lighter regions represent more heavily mineralized section at the time of diet switch.

($\delta^{13}C_{diet1} = -17‰$), plateau at about $-3 \pm 0.5‰$, whereas V3 and V5, whose new diet had 89% C_4 carbon ($\delta^{13}C_{diet2} = -13.4‰$), plateau at a higher $\delta^{13}C$ value of approximately -0.5 ± 0.5 ‰. These results indicate a 13‰ to 14‰ enrichment of ^{13}C in the apatite compared to the diet, consistent with earlier results (Lee-Thorp et al., 1989; Cerling and Harris, 1999).

Introduction of C_4 plants into the steer's diet is also recorded across the enamel thickness, as increasing $\delta^{13}C$ values from inner to outer enamel are found in high-resolution profiles (Table 2, Fig. 3). The largest isotopic difference between inner and outer enamel is observed in V3M2–4 (8.0‰), whereas the smallest is observed lower in the tooth in V3M2–6 (0.5‰). Enamel in V3M2–6 was likely formed after the diet switch, as suggested by high $\delta^{13}C$ values across the profile. Inner enamel from the upper 30–35 mm of the crown exhibits $\delta^{13}C$ values between $-13.2‰$ and $-6.7‰$. Isotope mass balance calculation shows that ~50% or more of the apatite was formed in this zone before the diet switch. Outer enamel has the highest $\delta^{13}C$ values, ranging between $-6.6‰$ and $+0.3‰$, suggesting that surface enamel was mostly mineralized after the diet switch. The total isotopic range in V3M2 is 13.5‰ with the high resolution technique, and only 11.5 ‰ with the conventional technique. Therefore, we can conclude that the conventional sampling strategy underestimates the amplitude of the isotopic shift that was recorded during the dietary change by ~15% compared to our microsampling strategy.

Measurement of carbonate contents ($[CO_3^{2-}]$) in individual subsamples highlights another feature of enamel crystallites (Table 2, Fig. 4). $[CO_3^{2-}]$ values decrease by ~2 wt% from the enamel dentine junction to the enamel surface. This difference indicates that inner and outer enamel apatite have different crystallographic properties because carbonate content in apatite controls the shape and size of the crystals (LeGeros and LeGeros, 1984). Well crystallized crystals containing fewer $[CO_3^{2-}]$ ions are located on the tooth surface, providing the tooth with a better resistance to external chemical and physical attacks.

4. DISCUSSION

4.1. Timing and geometry of mineralization in bovine enamel

We developed a two-dimensional map of V3M2 mineralization sequence based on the high-resolution profiles (Fig. 5A). $\delta^{13}C$ values from each profile are used to calculate the fraction of enamel mineralized after the diet switch. Pre-diet-switch $\delta^{13}C$ values are recorded in the innermost layer from the upper part of the crown, whereas $\delta^{13}C$ values post-diet-switch are found in the outer layer from the lower part of the crown. Therefore, the mineralization gradient can be deconvolved into a vertical component, from apex to cervix, and a horizontal component, from EDJ to outer enamel. $\delta^{13}C$-value isolines indicate that the mineralization front runs diagonally through the enamel thickness, extending outward from the EDJ at a relatively low angle.

We can use our dataset to determine the mineralization parameters for bovines (Fig. 5B) as defined by Passey and Cerling (2002). In their model, the authors assume constant

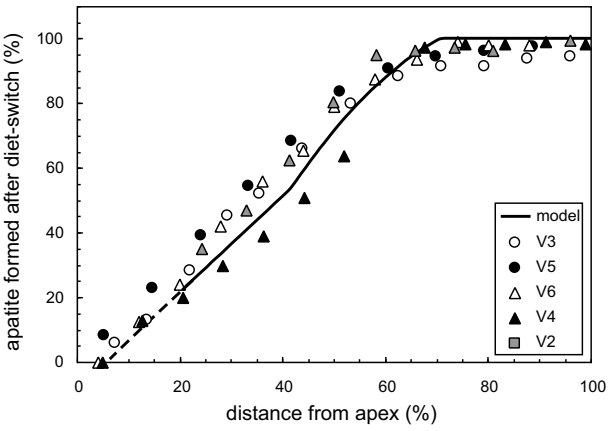

Fig. 6. Comparison between measured and modeled carbon isotope profiles in experimental steer, assuming $f_i = 0.25$. $\delta^{13}C$ values are expressed as the percent of apatite synthesized after the diet switch. End-member values are calculated from known dietary inputs, assuming ε_{AD} (+13.5‰). For individual V4, values exceeding 100% were calculated, and we used the highest $\delta^{13}C$ value of the profile as an estimate of 100% C_4. The profile from individual V2 was out of phase and shifted by 10 mm to fit the other profiles.

appositional length (l_a), an initial mineral content (f_i) during the stage of matrix formation, constant maturation length (l_m), constant growth rate, and a linear increase in mineral content ($1 - f_i$) during the stage of maturation. Maturation is achieved in a single step, with the mineralization wave running from the innermost layer toward the surface layer, such that no angular disparity between the two fronts can be found. The isotope value of each small volume i, oriented parallel to the appositional surface, can be calculated using the following equation (Passey and Cerling, 2002):

$$\delta_{ei} = (f_i \times \delta_{mi}) + (1 - f_i) \times \frac{\sum_{n=i+1}^{i+1+l_m} \delta_{mn}}{l_m} \quad (1)$$

where δ_{ei} is the isotope value of the fully mineralized enamel, δ_{mi} is the isotope value recorded in enamel during matrix apposition stage, and i is a submultiple of l_m. The isotope value of a column of enamel drilled perpendicular to the growth axis and spanning the enamel thickness is modelled by the following equation (Passey and Cerling, 2002):

$$\delta_{ci} = \frac{1}{l_a} \sum_{n=i-l_a}^{i} \delta_{en} \quad (2)$$

where δ_{ci} is the isotope value of each column of enamel.

In bovines, M2 starts to form when the animal is one month old (day 30), and ends one year later (day 395) (Brown et al., 1960). If we assume a constant growth rate for enamel, and considering an average tooth length of 50 mm, between 130 and 140 μm of new material is added daily along the appositional surface. At the time of the diet switch (day 295), the appositional front contacts the EDJ ~35 mm from the apex. On the same day, the appositional front should contact the external surface of the tooth just before this zone starts to exclusively record the new diet. This zone is located between tooth slices

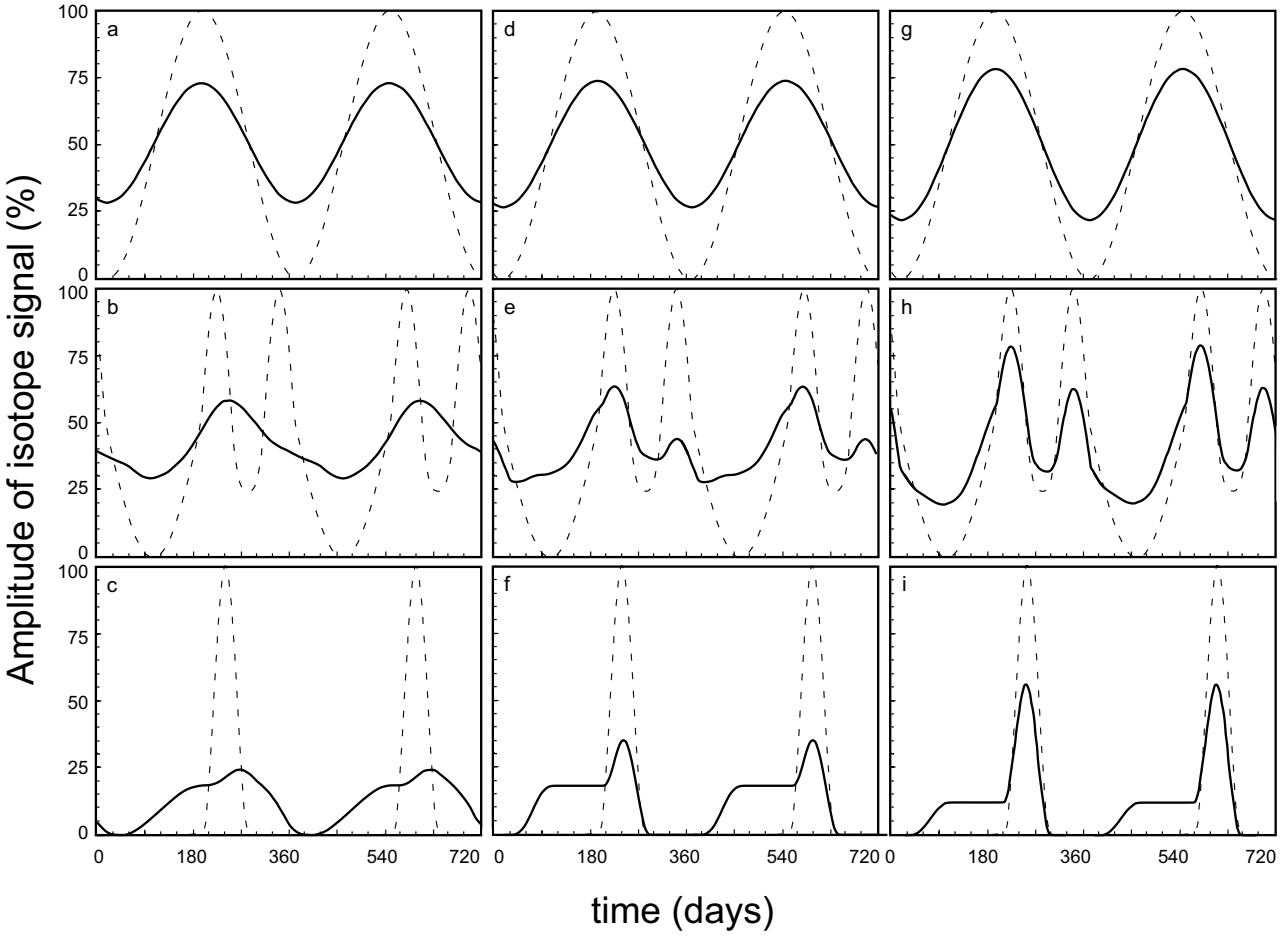

Fig. 7. Numerical simulation of isotopic variations recovered from a bovine second molar (solid lines) following three different sampling protocols. First column (a–c): Individual subsamples are milled perpendicular to the growth axis, across the entire enamel thickness. Second column (d–f): Individual subsamples are milled parallel to the appositional front, across the entire enamel thickness. Third column (g–i): Only the innermost enamel layer is sampled. Tooth enamel signals were modelled assuming $f_i = 0.25$ for (a–f) and $f_i = 0.5$ for (g–i) and for three different input signals (dashed lines): first line (a, d, g) sinusoidal, second line (b, e, h) quasisinusoidal with biannual 90 d excursions, and third line (c, f, i) synthetic with annual 90 d excursion from baseline.

3 and 4, ~20 mm from the top of the crown. Therefore, l_a is ~15 mm long. This value is identical to that measured for hippos by Passey and Cerling (2002). Maturation length l_m, which is the distance between the two portions of enamel recording the first and the second diet, is equal to ~25 mm. Assuming a constant growth rate, l_a and l_m are equivalent to 110 d and 183 d, respectively. The number assigned for l_m is in agreement with the estimation by Balasse (2002) for completion of enamel mineralization (6 to 7 months).

The predictions of the model are plotted against the isotope dataset for the five steers (Fig. 6), assuming $f_i = 0.25$ (Passey and Cerling, 2002). All individuals but one (V4) show very similar isotopic trends, that are successfully reproduced by the model. A somewhat slower increase in $\delta^{13}C$ values is recorded in the upper two-thirds of individual V4, a pattern that could be explained by a higher initial mineral content during matrix apposition. Enamel maturation has been described as a multistage process (Suga, 1982). Although more complex feeding experiments are needed to fine-tune the model, agreement between Passey and Cerling's model for ever-growing teeth and our data suggests that model assumptions are appropriate and can be used to predict isotopic attenuation of environmental signals in hypsodont teeth.

4.2. Implications for Isotope Attenuation: Toward a New Microsampling Strategy?

We modeled the isotopic attenuation resulting from different bovine tooth sampling strategies and input signals. Sinusoidal waves are usually thought to be the most representative function to describe environmental signals. For example, they can be used to model annual variations in $\delta^{18}O$ values of meteoric water ($\delta^{18}O_w$) in high- and midlatitudes sites (Dansgaard, 1964). Although non-sinusoidal variation is common in nature, an exhaustive review of environmental signals is beyond the scope of this paper. For this reason, we will restrict our discussion to examples presented in Passey and Cerling (2004): (1) The first example consists of a baseline with a single excursion lasting for three months; (2) the

second example is a quasisinusoidal signal, but with biannual excursions lasting three months each. This type of input signal can be used to model biannual rainy seasons in eastern Africa and the corresponding rise of C_4 plants. It can also model the amount effect (Dansgaard 1964) that takes place at low-latitude locations and consists of a marked decrease in $\delta^{18}O_w$ values subsequent to summer rains.

4.2.1. Sampling perpendicular to the growth axis

Figure 7a–c represents the signal obtained in bovine enamel when samples are milled following the conventional method. We assume that each subsample is milled perpendicular to the growth axis across the whole enamel layer and is ~130 μm thick, which corresponds to daily growth rate. Modelled curves are computed using Eqns. 1 and 2. A significant degree of damping is observed compared to the input signals. Isotopic attenuation increases with decreasing wavelength of the input signal, from 56% in the case of a sinusoidal signal (Fig. 7a) to 76% in the case of yearly excursion (Fig. 7c). Even more importantly, this sampling strategy is blind to the structure of the signal: Nonsinusoidal signals give rise to measured signals that appear sinusoidal (Fig. 7b and c). Although the conventional sampling strategy has been widely adopted for its convenience, we conclude that it cannot be used to infer details of past environmental signals recovered from bovine teeth unless the structure and wavelength of the input signal are known.

4.2.2. Sampling parallel to the appositional front

An alternative sampling strategy consists of micromilling subsamples parallel to the apposition front (oblique to the growth axis). This can be achieved by milling along Retzius lines generated each week during matrix apposition (Wiedemann 2000). Modelled curves are computed using Eqn. 1, assuming each subsample is ~130 μm thick (Fig. 7d–f). This sampling strategy clearly fails to recover the full record of environmental variability, but we notice some improvement relative to conventional sampling. Signals are dampened 49% instead of 56% in the case of a sinusoidal signal (Fig. 7d). Dampening reaches 58% and 65% in the case of nonsinusoidal signals (Fig. 7e and f), instead of 71% and 76% if one follows a conventional sampling strategy. Although recovery has improved compared to conventional sampling, it remains limited. For example, a sinusoidal signal with an amplitude of 5‰ will translate to a difference of 0.35‰ between the two sampling strategies, which is very close to the reproducibility of the measurements (±0.1‰–0.3‰ depending on the techniques). This strategy also fails to recover the structure of nonsinusoidal input signals, although some improvement is apparent relative to conventional sampling (Fig. 7e and f).

4.2.3. Sampling at the enamel-dentine junction

Balasse (2003) suggested the microsampling of the innermost enamel layer as a potential alternative strategy. This zone is more heavily mineralized than any other layer during the stage of matrix deposition (Suga, 1982), thereby limiting the damping of isotopic signatures. Densitometry of microradiography of rat incisor enamel suggests that mineralization is 56% complete after the deposition of the organic matrix (Suga, 1979). There is no quantitative estimate of f_i at the innermost enamel layer available for bovines, but quantitative microradiography of unerupted bovine enamel suggests that calcification is between 40% and 57% for this zone (see Figs. 1 and 3 in Sakae and Hirai, 1982). Curves are computed using Eqn. 1, assuming that $f_i = 0.5$ (Fig. 7g–i). This strategy permits a significant improvement in recovery of the primary sinusoidal and nonsinusoidal variation. It is now possible to satisfactorily reproduce the structure of nonsinusoidal variability (Fig. 7h). Even more interesting is the fact that the isotopic damping measured at the EDJ remains constant (42% to 44%), independent of the structure of the environmental signal. Therefore it remains possible to reconstruct the amplitude of the environmental signal recorded in fossil enamel even if the true structure of this signal remains unknown, merely by magnifying the recovered isotope variability. This alternative strategy seems promising, yet it remains challenging for two primary reasons: (1) Experimental background work will be required to precisely estimate f_i values for a variety of different species, and (2) new microsampling protocols have to be designed to extract the innermost enamel layer. Although there is currently no estimate for bovine enamel, this zone was estimated to be ~10 μm thick in goat and sheep enamel (Suga, 1982). This is much thinner than the precision of laser ablation methods (100 ± 100–200 μm, Sharp and Cerling, 1996, 1998), but within the limits of the micromilling technique (Wurster et al., 1999). We evaluated the validity of our sampling protocol by comparing the dietary change measured at the EDJ along the tooth height of V3M2, with the predicted change modeled using Eqn. 1 (Fig. 8). Although our sampling protocol was not initially designed to isolate the innermost enamel layer, our data set is in reasonably good agreement with the predictions of the model as it successfully reproduces first-order trends. The most salient feature of this curve (i.e., the dramatic change predicted in the lower third of the crown) is reproduced by a rapid switch between V3M2–5 and V3M2–6, and all micromilled subsamples but one (in V3M2–3) are less than 15% off the modelled line. However, $\delta^{13}C$ values from subsamples located in

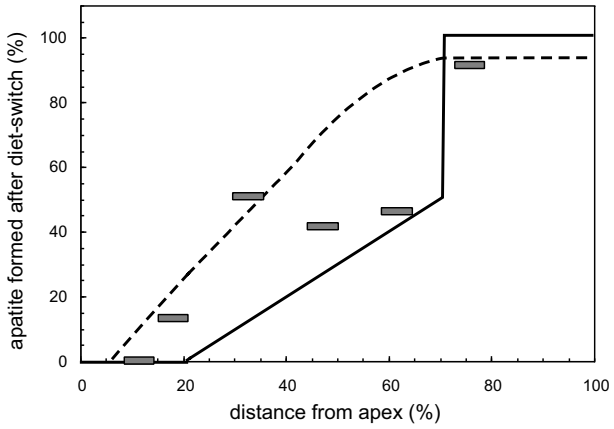

Fig. 8. Comparison between measured (gray boxes) and modeled (solid line) carbon isotope composition close to the EDJ in individual V3. The $\delta^{13}C$ values corresponding to the innermost subsample of each tooth profile are compared to a modeled curve obtained using Eqn. (1) and assuming $f_i = 0.5$. Intratooth variations measured using the conventional sampling strategy (dotted line) are shown for comparison. All $\delta^{13}C$ values are expressed as the percent of apatite synthesized after the diet switch.

the upper tooth slices show an excessive contribution of the C_4-dominant diet, a feature that could be explained by a mixing between the innermost and adjacent enamel layers. Therefore, an ideal sampling protocol remains to be found to test our hypothesis. The challenge will be to physically isolate the innermost enamel from the overlying enamel and underlying dentine, while collecting enough material for isotope analysis.

5. CONCLUSION

For the first time, high-resolution carbon isotope profiles have been generated within the enamel thickness using micromilling techniques. Our sampling strategy has been demonstrated as capable of identifying large variation in $\delta^{13}C$ values (up to 8‰) within a single tooth slice, corresponding to the diet-switch experienced by a steer during tooth growth. Increasing $\delta^{13}C$ values were found from the top of the crown to the root, and from the enamel-dentine junction to the outer enamel. Downward and outward increasing contribution of C_4 food to the enamel $\delta^{13}C$ values document the vertical and horizontal components of the mineralization gradient. Using this methodology, we determined Passey and Cerling (2002) model parameters for bovines and calculated expected isotopic damping for an array of theoretical environmental inputs and sampling strategies. Although popular in paleoclimate studies, the conventional sampling strategy results in large isotopic damping that is dependent in part on the structure of the environmental input signal. Therefore, investigation of changes in seasonal amplitudes of environmental signals recorded in tooth enamel is only possible if individuals from the same species are compared, and requires a reasonable knowledge of the structure of the input signal. Instead, we propose an alternative sampling strategy, restricted to the innermost enamel layer localized at the enamel-dentine junction. This strategy might offer the advantage of significantly reducing the isotope damping that would then be independent of the structure of the input signal. Additional technical adjustments will be required to test the predictions of the model.

Acknowledgments—We would like to thank Elise Dufour, Tim Prokopiuk, Blaine Novakovski, and Chris Wurster for technical assistance at different stages of this research. We also express appreciation to Bruce Eglington, Chris Holmden, and Chris Wurster for constructive comments of an earlier version of the manuscript. We also wish to acknowledge D. R. Cole, B. H. Passey, D. L. Fox, and an anonymous reviewer for their thorough reviews. This research was supported by a grant from the Fondation Singer-Polignac to Antoine Zazzo and a CNRS ACI "jeunes chercheurs " grant #67053.

Associate editor: David Cole

REFERENCES

Balasse M. (2002) Reconstructing dietary and environmental history from enamel isotopic analysis: Time resolution of intra-tooth sequential sampling. *Int. J. Osteoarchaeol.* **12,** 155–165.

Balasse M. (2003) Potential biases in sampling design and interpretation of intra-tooth isotope analysis. *Int. J. Osteoarchaeol.* **13,** 3–10.

Balasse M., Bocherens H., and Mariotti A. (1999) Intra-bone variability of collagen and apatite isotopic composition used as evidence of a change of diet. *J. Arch. Sci.* **26,** 593–598.

Balasse M., Bocherens H., Mariotti A., and Ambrose S. H. (2001) Detection of dietary changes by intra-tooth carbon and nitrogen isotopic analyses: an experimental study of dentine collagen of cattle (*Bos taurus*). *J. Arch. Sci.* **28,** 235–245.

Balasse M., Ambrose S. H., Smith A. B., and Price T. D. (2002) The seasonal mobility model for prehistoric herders in the south-western Cape of South Africa assessed by isotopic analysis of sheep tooth enamel. *J. Arch. Sci.* **29,** 917–932.

Brown W. A. B., Christofferson P. V., Massler M., and Weiss M. B. (1960) Postnatal tooth development in cattle. *Am. J. Vet. Res.* **21,** 7–34.

Dansgaard W. (1964) Stable isotopes in precipitation. *Tellus* **16,** 436–468.

Cerling T. E. and Harris J. M. (1999) Carbon isotope fractionation between diet and bioapatie in ungulate mammals and implications for ecological and paleoecological studies. *Oecologia* **120,** 247–263.

Fisher D. L. and Fox D. C. (1998) Oxygen isotopes in mammoth teeth: sample design, mineralization patterns and enamel-dentine comparisons. *J. Vert. Pal.* **18,** 41A–42A.

Fricke H. C. and O'Neil J. R. (1996) Inter- and intra-tooth variation in the oxygen isotope composition of mammalian tooth enamel phosphate: implications for palaeoclimatological and palaeobiological research. *Palaeogeogr. Palaeoclimatol. Palaeoecol.* **126,** 91–99.

Gadbury C., Todd L., Jahren A. H., and Amundson R. (2000) Spatial and temporal variations in the isotopic composition of bison tooth-enamel from the Early Holocene Hudson-Meng Bone Bed, Nebraska. *Palaeogeogr. Palaeoclimatol. Palaeoecol.* **157,** 79–93.

Hoppe K. A., Stover S. M., Pascoe J. R., and Amundson R. (2004) Tooth enamel biomineralization in extant horses: implications for isotopic microsampling. *Palaeogeogr. Palaeoclimatol. Palaeoecol.* **206,** 355–365.

Kohn M. J., Schoeninger M. J., and Valley J. W. (1998) Variability in oxygen compositions of herbivore teeth: reflections of seasonality or developmental physiology? *Chem. Geol.* (*Isot. Geosci. Sect.*) **152,** 97–112.

Lee-Thorp J. A., Sealy J. C., and van-der-Merwe N. J. (1989) Stable carbon isotope ratio differences between bone collagen and bone apatite and their relationship to diet. *J. Arch. Sci.* **16,** 585–599.

LeGeros R. Z. and LeGeros J. P. (1984).Phosphate minerals in human tissues. In *Phosphate minerals* (eds. J. O. Nriagu and P. B. Moore), pp. 352–385. Springer-Verlag.

Moss-Salentijn L., Moss M. L. and Yuan M. S. (1997) The ontogeny of mammalian enamel. In *Tooth enamel microstructure* (eds. W. V. Koeningswald and P. M. Sander), pp. 5–30. A. A. Balkema.

Passey B. H. and Cerling T. E. (2002) Tooth enamel mineralization in ungulates: Implications for recovering a primary isotopic time-series. *Geochim. Cosmochim. Acta* **66,** 3225–3234.

Passey B. H. and Cerling T. E. (2004) Response to the comment by M. J. Kohn on "Tooth enamel mineralization in ungulates: Implications for recovering a primary isotopic time-series," by B. H. Passey and T. E. Cerling (2002). *Geochim. Cosmochim. Acta* **68,** 407–410.

Sakae T. and Hirai G. (1982) Calcification and crystallization in bovine enamel. *J. Dent. Res.* **61,** 57–59.

Sharp Z. D. and Cerling T. E. (1996) A laser GC-IRMS technique for in situ stable isotope analyses of carbonates and phosphates. *Geochim. Cosmochim. Acta.* 60:2909–2916.

Sharp Z. D. and Cerling T. E. (1998) Fossil isotope records of seasonal climate and ecology: Straight from the horse's mouth. *Geology* **26,** 219–222.

Suga S. (1979) Comparative histology of progressive mineralization pattern of developing incisor enamel of rodents. *J. Dent. Res.* **58,** 1025–1026.

Suga S. (1982) Progressive mineralization pattern of developing enamel during the maturation stage. *J. Dent. Res.* **61,** 1532–1542.

Suga S., Murayama Y., and Musashi T. (1970) A study of the mineralization process in the developing enamel of Guinea pigs. *Arch. Oral Biol.* **15,** 597–612.

Suga S., Aoki H., Yamashita Y. Tsuno M., and Ogawa M. (1987) A comparative study of disturbed mineralization of rat incisor enamel induced by strontium and fluorine administration. *Adv. Dent. Res.* **1,** 339–355.

Weinmann J. P., Wessinger G. D., and Reed G. (1942) Correlation of chemical and histological investigations on developing enamel. *J. Dent. Res.* **21,** 171–182.

Wiedemann F. B. (2000) Experimental data on enamel desposition in sheep: Implications for sampling strategies for stable isotope analyses. *J. Hum. Evol.* **38,** A34.

Wurster C. M., Patterson W. P., and Cheatham M. M. (1999) Advances in micromilling techniques: A new apparatus for acquiring high-resolution oxygen and carbon stable isotope values and major/minor elemental ratios from accretionary carbonate. *Comput. Geosci.* **25,** 1159–1166.

Zazzo A., Mariotti A., Lécuyer C., and Heintz E. (2002). Intra-tooth isotopic variations in Late Miocene bovid enamel from Afghanistan: Paleobiological, taphonomical and climatical implications. *Palaeogeogr. Palaeoclimatol. Palaeoecol.* **186,** 145–161.